Determination of Pore Size Distribution, Surface Area, and Acidity in Fluid Cracking Catalysts (FCCs) from Nonlocal Density Functional Theoretical Models of Adsorption and from Microcalorimetry Methods

Mario L. Occelli,*,† James P. Olivier,‡ Alice Petre,§ and Aline Auroux§

MLO Consulting, 6105 Black Water Trail, Atlanta, Georgia 30328; Micromeritics Instrument Corp., Inc., Norcross, Georgia 30093; and Institut de Recherches sur la Catalyse, CNRS, 2 Av. A. Einstein, 69626 Villeurbanne, France

Received: October 17, 2002; In Final Form: February 5, 2003

A method based on nonlocal density functional theory (NLDFT) has been used to interpret the data for the adsorption of nitrogen at 77 K within the pores of three different commercial fluid cracking catalysts (FCCs) before and after their use in a refinery catalytic cracking unit. The integral equation of adsorption was inverted by a regularization method to yield the micropore and mesopore size distribution over a wide range of pore widths. The results obtained are compared with the results of more traditional data treatments and indicate that the NLDFT model can provide a realistic pore volume and surface area estimation in commercial FCCs irrespective of their chemical composition and pore width distribution. Both BET and Langmuir methods grossly underestimate the FCCs surface area, and only the NLDFT method yields reliable surface area and pore volume measurements over the entire micro−meso porosity range present in the catayst under study. Adsorption microcalorimetry results using ammonia as a probe molecule reveal that as long as Lewis acid sites with strength greater than 100 kJ/mol are present and as long as these sites are available to gas oil, FCCs can retain their useful cracking activity and selectivity properties.

Introduction

In all modern refineries, the fluid catalytic cracking unit (FCCU) remains the major means of gasoline production. In a FCCU heavy oil feedstocks are converted (cracked) into high-value liquids such as gasoline and heating oil in the presence of a fluid cracking catalyst (FCC) operating at temperatures in the 480−550 °C range. Following the cracking reaction, the spent catalyst is first exposed to steam (480−540 °C) to remove occluded hydrocarbons, and then it is sent to the regenerator where coke deposits are removed by heating in air at temperatures in the 600−700 °C range. The regenerated FCC is then ready to be recycled to the FCCU reaction zone (the riser). Easy accessibility of active sites in the internal porosity of fluid cracking catalysts is essential to the efficient and selective cracking of gas oils to gasoline and other valuable products.

The conventional approach to study porosity losses and structural changes suffered by FCCs during the thermal and hydrothermal treatments encountered in a FCCU is to monitor the reduction of surface area (SA) and pore volume (PV) by nitrogen porosimetry experiments using traditional methods.[1,2] The Kelvin equation has been routinely used to correlate pore size to the pressure at which condensation of the probe molecule in the pores takes place. Although it can be considered exact in the large pore limit, its accuracy decreases drastically as the pore width approaches molecular dimensions. For solids void of micropores the Barret−Joyner−Halenda (BJH) method[3] is frequently used. The Langmuir[4] and Brunauer−Emmett−Teller (BET)[5] formalisms are based on the model of adsorption on a free surface. The Langmuir model assumes the surface saturates after the first adsorbed layer, while the BET model presumes that multilayers can form at higher pressures. However, neither model allows for the filling of micropores. Thus, surface areas derived from these two models will differ from the actual area in a way that depends on the solid's porous structure.

The determination of pore size distribution in microporous solids has been studied in the past using the Dubinin−Radushkevich (DR) method,[6] *t*- or α-plots,[7,8] and MP[9] methods, to name a few. The Horvath−Kawazoe (HK) procedure[10] is a method of calculating the effective micropore size distribution of slit-shaped pores in carbons from adsorption isotherms; the HK theory has also been extended to cylindrical pores.[11] However, the assumptions on which the HK method is based have been recognized as flawed.[12]

In a companion paper,[13] we have shown the utility of a hybrid density functional model to describe the porosity of pillared clay catalysts. That model specifically incorporates the characteristics of the smectite surface and is not appropriate for the zeolite-based materials considered here. It is the purpose of this paper to report the loss of acidity and porosity experienced by three different commercial zeolite-based FCC samples during gas oil cracking in a refinery FCCU using a nonlocal density functional theory (NLDFT) model.[14,15] This model is better suited to describing the pore space of a zeolite. Surface area and pore volume distribution will be investigated with traditional equations and compared with results obtained with NLDFT. The BJH method was not considered, since typical commercial FCCs are mainly microporous solids.[16] Acidity will be determined from adsorption microcalorimetry experiments using ammonia as the probe molecule.[17−19]

† MLO Consulting. E-mail: mloccell@mindspring.com.
‡ Micromeritics Instrument Corp., Inc. E-mail: jolivier@ micromeritics.com.
§ Institut de Recherches sur la Catalyse. E-mail: aline.auroux@ catalyse.univ-lyon1.fr.

10.1021/jp022242m CCC: $25.00
Published on Web 04/03/2003

TABLE 1: Elemental Analyses for Some Commercial FCC Samples before and after Use in a Refinery FCCU[a]

	fresh FCCs			equilibrium FCCs		
	A	B	C	A	B	C
Al_2O_3 (wt %)	36.7	51.6	50.5	37.0	51.8	52.6
CaO (wt %)	0.042	0.070	0.084	0.060	0.080	0.045
MgO (wt %)	0.016	0.033	0.050	0.10	0.04	0.11
C (wt %)				0.04	0.13	0.52
Fe (wt %)	0.27	0.38	0.40	0.46	0.59	0.45
Na (wt %)	0.29	0.25	0.25	0.27	0.36	0.28
TiO_2 (wt %)	0.60	0.90	0.95	1.06	1.13	1.29
P_2O_5 (wt %)	0.13	0.13	0.13	0.19	0.06	0.06
RE (wt %)	2.07	2.25	2.50	1.89	2.38	2.62
Cu (ppm)				19.5	20.0	37.5
Ni (ppm)				3586	4732	587
V (ppm)				2885	3169	334
Sn (ppm)				37.5	11.0	16.5
Sb (ppm)				690	1935	7.0

[a] %RE = %Ce + %La + %Nd + %Pr.

TABLE 2: Some Microactivity Test Results for the Three Commercial Equilibrium FCCs under Study[a]

	FCC-A	FCC-B	FCC-C
conversion (wt %)	70.7	71.1	78.1
gasoline (wt %)	45.3	47.5	50.5
LCGO (wt %)	16.2	17.8	14.1
SO (wt %)	13.1	11.1	7.8
carbon (wt %)	5.08	5.00	4.78
hydrogen (wt %)	0.60	0.47	0.16

[a] A reactor temperature of 537 °C and a C/O = 3.0 were used. Material balance ~ 99%.

Experimental Section

Materials. The three commercial FCCs under study are microspheres containing kaolin and an HY type zeolite stabilized with low levels of rare earth (RE) cations (Table 1). Specifically, FCC-A microspheres contain ~30 wt % zeolite, and their matrix is an aluminosilicate gel. In contrast, samples FCC-B and FCC-C contain only ~20 wt % zeolite, and their matrix is an alumina gel that imparts a high (>50%) Al content to the catalysts. Chemical analysis of the three fresh FCCs and of their equilibrium counterpart is in Table 1.

Microactivity Testing (MAT). Microactivity testing (MAT) of the equilibrium FCC samples was conducted with a Kuwait vacuum gas oil (VGO) and a reactor temperature of 537 °C, using a 60 s injection time and a cat/oil (C/O) ratio of ~3.0. The VGO used contained 0.103 wt % total nitrogen and 3.1 wt % total sulfur. The equilibrium FCCs were obtained from different U.S. refineries. MAT results are in Table 2.

Surface Area Analysis. Nitrogen sorption isotherms obtained at liquid nitrogen temperature were collected using a volumetric technique on a Micromeritics ASAP 2010 adsorption instrument. Prior to analysis, samples weighing from 0.1 to 0.3 g were outgassed in a vacuum at 400 °C overnight. DFT Plus software (from Micromeritics) was used to calculate surface areas and pore size distributions, using the models and techniques described below.

Results and Discussion

Materials. Elemental analysis results are in Table 1. Inspection of these data indicates that the fresh FCCs contain minor amounts of iron and titania (probably rutile) impurities associated with the clay (kaolin) used in catalyst preparation. All the samples contain a low level of phosphorus, a residual impurity possibly resulting from the use of tetrasodium pyrophosphate (TSPP) to delaminate the clay during catalyst preparation. The FCCUs, in which the catalysts have been used, crack metal contaminated gas oil. Thus, during gas oil cracking, metals have been deposited on all the three catalysts, generating equilibrium FCCs containing Ni and V impurities in the 580−3600 and 330−3200 ppm ranges, respectively; see Table 1. Vanadium irreversibly decreases the crystallinity of the HY type zeolite and with it the catalyst activity. In contrast, nickel has no effect on activity but catalyzes the secondary cracking of the gasoline produced, generating light gases and coke; metal effects on FCCs' performance have been reviewed elsewhere.[20] In the case under study, the refiner has chosen to mitigate the deleterious effects of Ni and V by adding Sb (to passivate Ni) and Sn (to passivate V) compounds to the FCCU. As a result, all the equilibrium FCCs retain their useful cracking activities and gasoline selectivity; see Table 2. In fact, the high (>6000 ppm (Ni + V)) metal levels in samples FCC-A and FCC-B have been passivated by the addition of Sb and Sn compounds at the concentrations indicated in Table 2. Although containing only 20% zeolite the low (<1000 ppm (Ni + V)) metal levels provides sample FCC-C with a cracking activity higher than the one exhibited by FCC-A containing 30% zeolite, gasoline/conversion and coke/conversion ratios do not change greatly and remain in the 0.60−0.70 and 0.060−0.072 ranges, respectively (Table 2). An equilibrium FCC is a catalyst whose properties have become invariant with time.

Density Functional Theory (DFT) Method. The density functional theory (DFT) formalism has in recent years received considerable attention as a way to describe the adsorption process at a gas/solid interface of pores with slitlike or cylindrical geometry.[21] The ability of DFT to model physical adsorption provides a novel method to extract surface area and pore size distribution results from experimental adsorption isotherms.[22]

The density functional approach to understanding the structure of inhomogeneous fluids at a solid interface consists of constructing the grand potential functional, $\Omega[\rho(\mathbf{r})]$, of the average singlet density, $\rho(\mathbf{r})$, and minimizing $\Omega[\rho(\mathbf{r})]$ with respect to $\rho(\mathbf{r})$ to obtain the equilibrium density profile and thermodynamic properties:

$$\Omega[\rho(\mathbf{r})] = F[\rho(\mathbf{r})] + \int \mathrm{d}r\, \rho(\mathbf{r})[V_{\mathrm{ext}}(\mathbf{r}) - \mu_{\mathrm{b}}] \qquad (1)$$

where μ_{b} is the bulk chemical potential imposed on the system and $V_{\mathrm{ext}}(\mathbf{r})$ is the wall potential. At the equilibrium $\rho(\mathbf{r})$, the value of $\Omega[\rho(\mathbf{r})]$ will be a minimum. Thus, by differentiating eq 1 with respect to the density $\rho(\mathbf{r})$ and equating it to zero, it is possible, at least in principle, to solve the resulting equation for the equilibrium density profile $\rho(\mathbf{r})$ in pores of a certain width by an iterative numerical method once expressions for $F[\rho(\mathbf{r})]$ and $V_{\mathrm{ext}}(\mathbf{r})$ are known. The net quantity adsorbed at a given pressure is then found by integrating $\rho(\mathbf{r})$ from wall to wall and subtracting a quantity equivalent to the nonexcluded volume of the pore at the bulk gas density.

$$Q_{\mathrm{ads}} = \int \mathrm{d}z\, (\rho(z) - \rho_0(z)) \qquad (2)$$

The result is normalized to one square meter of wall area and expressed as cm^3 STP for direct comparison with experimental data. For solids having a distribution of pore sizes, the integral equation of isothermal adsorption becomes

$$Q(p) = \int \mathrm{d}H\, q(p,H)\, f(H) \qquad (3)$$

where $Q(p)$ is the total quantity of adsorbate per gram of adsorbent at pressure p; $q(p,H)$, the kernel function, describes

the adsorption isotherm for an ideally homoporous material characterized by pore width H as a quantity of adsorbate per square meter of pore surface, and $f(H)$ is the desired pore surface area distribution function with respect to H. The generation of an adsorption isotherm will require the application of eq 3 over the entire pressure range considered; the limits of integration in eq 3 will be between the molecular diameter of the probe molecule and infinity (a free surface). Using the set of NLDFT models constructed as described in detail elsewhere[23] and the experimental adsorption isotherm for the function $Q(\mathbf{p})$, eq 3 was solved for the distribution vector $f(H_i)$. It is then possible to extract pore size distribution data from experimental adsorption isotherms.[24,25] Examples of the resulting distributions of pore area and pore volume by pore width in porous heterogeneous catalysts are shown in the figures in this paper and elsewhere.[15,26]

Nitrogen Porosimetry Results. Previous investigations of the porous structure of FCCs have indicated that these catalysts are essentially microporous solids with most of their microporosity resulting from the presence of 20−30% HY type zeolite, the catalyst cracking component.[16] Nitrogen adsorption and porosimetry results in Figure 1 are consistent with previous results. The isotherms in Figure 1 are type II isotherms typical of solids having a bimodal distribution of pore widths (micro- and mesopores). After complete micropore filling near $P/P_0 = 0.1$, nitrogen uptake monotonically continues with increasing pressure, owing to nitrogen adsorption in the FCCs mesoporous structure (Figure 1). The larger nitrogen uptake at $P/P_0 = 0.1$ shown by FCC-A is attributed to the catalyst 30 wt % zeolite content; see Figure 1A. Near $P/P_0 = 0.90$, there is a sharp increase in nitrogen uptake probably due to nitrogen condensation in the larger mesopores The small parallel loop hysteresis observed in Figure 1 is typical of solids, such as FCCs, that contain slit-shaped mesopores resulting, in this case, from the presence of kaolin platelets. Slit-shaped pores on the surface of several commercial FCCs have been observed by atomic force microscopy.[27] However, 94% of the total DFT surface area is in pores with width below 1.0 nm, indicating that the FCC microporosity indeed originates in the HY type crystals present in the catalyst microspheres. Samples FCC-B and FCC-C, in addition to having an alumina matrix, contain only ∼20 wt % zeolite. As a result, the nitrogen uptake near $P/P_0 = 0.1$ is ∼70% the one observed in FCC-A (Figure 1B and C). In Figure 1, the near parallelism of the isotherms after micropore filling indicates that little change in the mesopore structure has occurred in equilibrium FCCs. The reduction in sorption capacity expressed by the three equilibrium FCCs in Figure 1 represents the losses of crystallinity resulting from the thermal and hydrothermal treatments required for catalyst regeneration and from the deleterious effects on zeolite stability induced by vanadium deposition during gas oil cracking in a FCCU. The same data are plotted on a semilog scale in Figure 2. It is seen that, in the very low-pressure region near $10^{-7}(P/P_0)$, nitrogen sorption is negligible in all three FCCs. Below a relative pressure of 10^{-1}, the equilibrium FCC samples show lower uptakes of nitrogen probably caused by microporosity losses resulting from a partial degradation of the HY structure and from the presence of metal impurities, see Table 1.[16]

The cumulative surface area and volume distribution in Figures 3 and 4 suggest that the aging process and metals' deposition affect mainly pores with a diameter smaller than 1.0 nm. The plot in Figure 3 more specifically indicates that the cumulative pore area in micropores results from nitrogen sorptions in pores with width below 1.0 nm and that the total

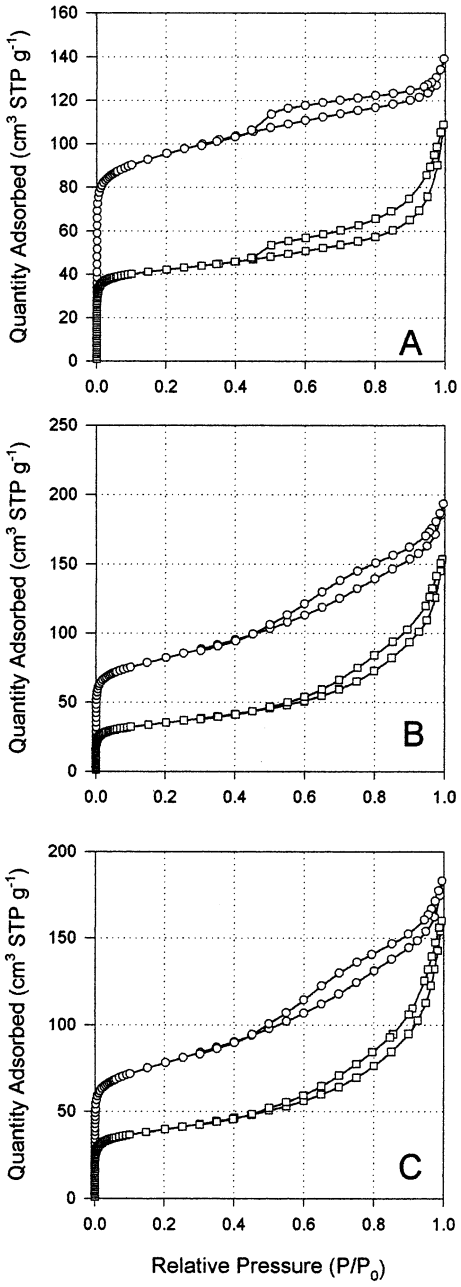

Figure 1. Nitrogen sorption isotherms at 77 K showing the DFT fitted results (solid line) for the fresh (top) and equilibrium (bottom) FCC sorption isotherms: (A) sample FCC-A; (B) sample FCC-B; (C) sample FCC-C.

area remains unchanged in the 1.0−2.0 nm range (Figure 3A). Between 2 and 4.0 nm there is a very small but noticeable increase in SA owing to the presence of a small population of mesopores (Figure 3A). Mesoporosity is more evident in FCC-B and FCC-C samples. In fact, after micropore filling, the SA remains constant in the 1.0−3.0 nm range, increases between 3.0 and 10 nm, and again becomes essentially constant for pore widths larger than 20 nm (Figure 3B and C). The same trend is also observed in the corresponding equilibrium samples. The greater increase in SA above 3.0 nm indicates that when aluminosilicates are replaced by alumina as the matrix, the resulting FCCs contain greater mesoporosity. Cumulative PV distribution data are in Figure 4. In this figure, the change in the cumulative pore volume in fresh and equilibrium FCCs is plotted as a function of pore width. As already noticed in Figure 3, the pore SA and PV rapidly increase for pore width < 1.0

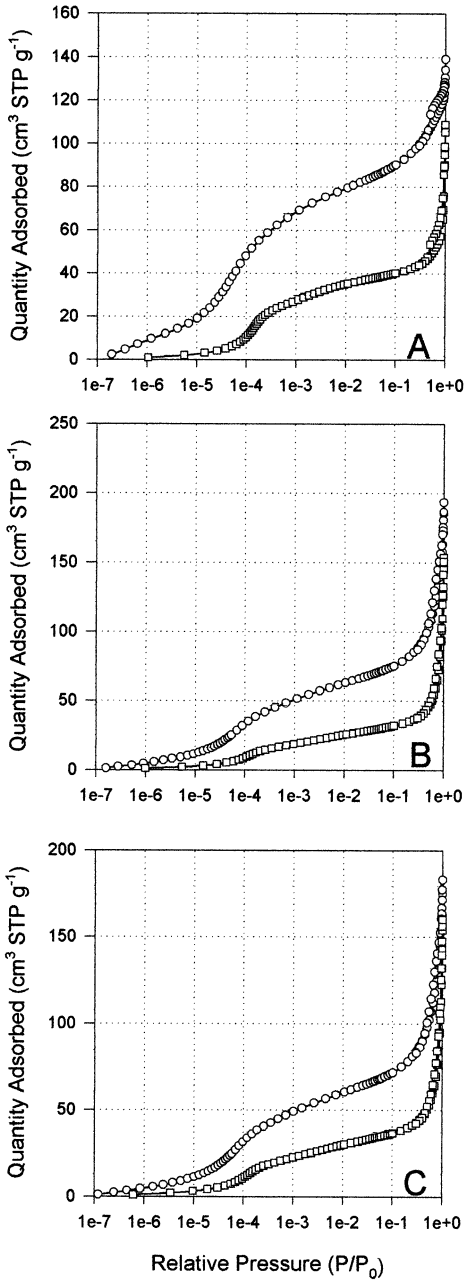

Figure 2. Nitrogen sorption isotherms at 77 K in the low-pressure region showing the DFT fitted results (solid line) for the fresh (top) and equilibrium (bottom) FCC sorption isotherms: (A) sample FCC-A; (B) sample FCC-B; (C) sample FCC-C.

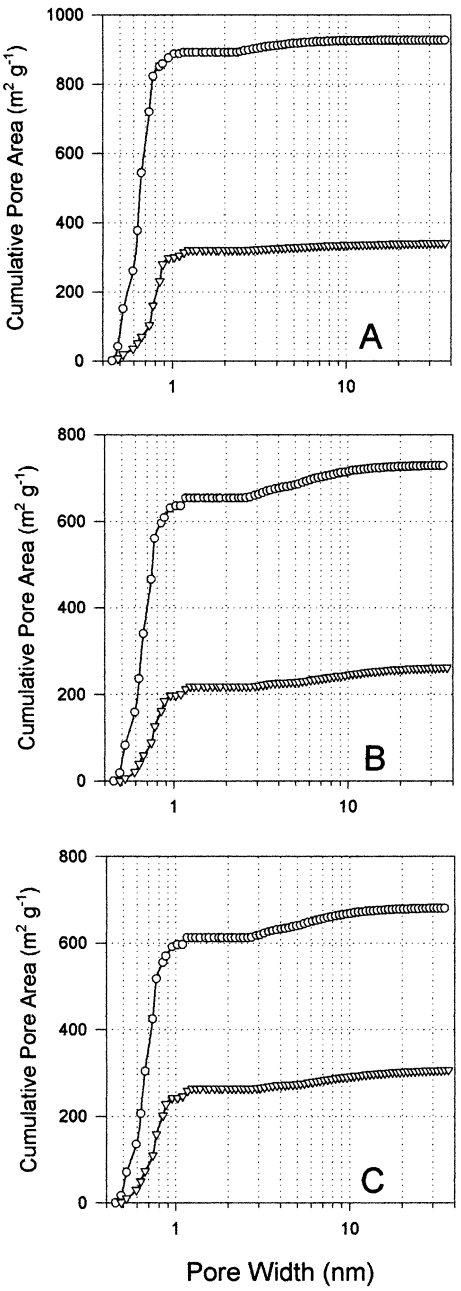

Figure 3. Cumulative pore area data obtained by fitting the DFT model to the fresh (top) and equilibrium (bottom) sorption isotherms: (A) sample FCC-A; (B) sample FCC-B; (C) sample FCC-C.

nm, owing to nitrogen sorption in the FCC acidic component (the zeolite). There is a smaller second increase in PV above 2.0 nm due to nitrogen uptake in the catalyst mesopores resulting from the clay platelets' agglomeration (Figure 4A). Mesopores are more evident in FCC-B and FCC-C samples, and above 2.0 nm, their cumulative PV monotonically increases with pore widths, owing to nitrogen sorption in voids resulting from the agglomeration of the FCC components (the kaolin, the zeolite, and its matrix) (Figure 4B and C). Crystallinity losses as well as metals' deposition and partial pore blockage are responsible for the decreased PV experienced by the equilibrium FCCs over the pore width range investigated; see Figure 4. Details of the effects of aging on catalyst porosity are better illustrated in Figure 5.

In Figure 5 differences in cumulative pore volume between the equilibrium and fresh FCCs as a function of pore width are plotted. This figure can be interpreted to indicate that micropores between 0.4 and 0.8 nm and some mesopores with pore width greater than 2.0 nm suffer a loss of volume owing to metals' (and coke) deposition. This trend is observed in all three FCCs under study. In FCC-A, in the 0.8−1.0 nm range, there is a small increase in PV that may be the result of narrowing of larger pores due to debris deposition on pore walls. Furthermore, it seems that when the catalyst contains an aluminosilicate matrix, pore widths in the 1.2−2.5 and 3.8−10 nm ranges are not affected by debris deposition during gas oil conversion. In contrast, for catalysts containing an alumina matrix, differences in cumulative pore volume for pore widths in the 2.8−10 nm range monotonically decrease (Figure 5). In all three FCCs, above 10 nm, differences in cumulative pore volume increase, possibly as the result of the collapse of larger mesopores. Since FCC-B and FCC-C samples have similar initial compositions (20% REHY and an alumina matrix) and generate equilibrium

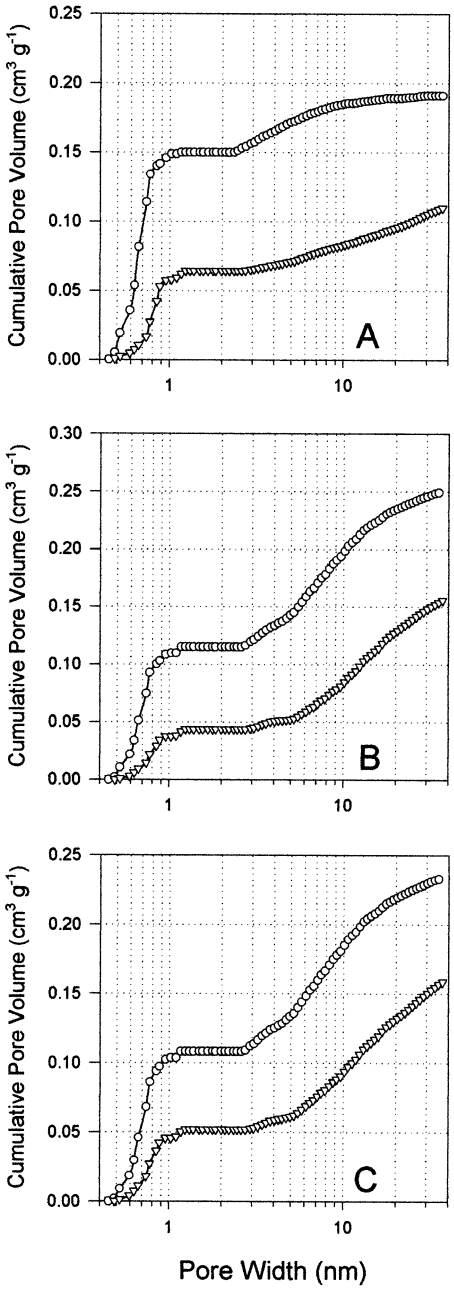

Figure 4. Cumulative PV distribution data obtained by fitting the DFT model to the fresh (top) and equilibrium (bottom) sorption isotherms: (A) sample FCC-A; (B) sample FCC-B; (C) sample FCC-C.

samples having different metals' levels, the larger losses in microporosity and mesoporosity seen in Figure 5 for sample FCC-B can be safely attributed to metals' (Ni, Sb, V, Sn, Cu, Fe) deposition on the FCC pore walls.

The incremental PV data shown in Figure 6 are consistent with the sorption isotherms in Figures 1 and 2 and with the SA and PV distribution data in Figures 3 and 4; that is, incremental PV is highest in the FCC sample containing the highest zeolite concentration. The micropores have pore widths < 1.0 nm and exhibit an average pore diameter near 0.74 nm (Figure 1A, C, and E), well in agreement with the effective pore opening of a zeolite with the faujasite structure. These results collectively indicate that, in a FCCU, metals' deposition and crystallinity losses affect mainly the equilibrium catalyst microspace while the mesoporosity present undergoes only minor changes and continues to provide access to the catalytically active microspace. The replacement of an aluminosilicate with an alumina

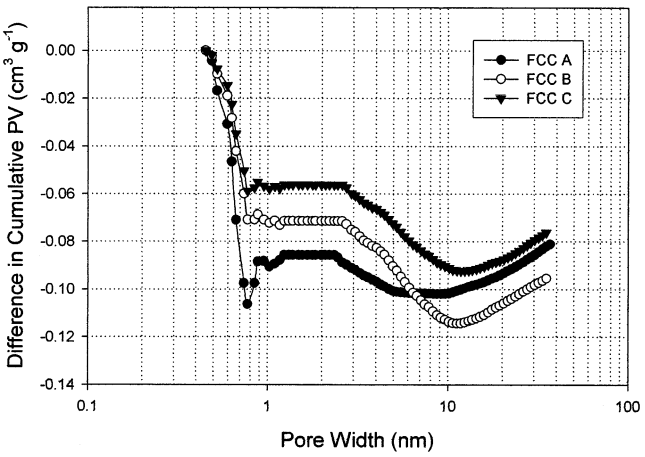

Figure 5. Cumulative PV difference between equilibrium and fresh FCC samples.

gel matrix results in catalysts having greater mesoporosity; see Figure 6B, D, and F.

In Tables 3−5, porosimetry results are compared to those of traditional methods. It can be seen that the BET and the Langmuir methods greatly underestimate the FCC surface area. BET surface areas in the range 100−200 m^2/g are typical values reported for FCCs. Values of 700-800 m^2/g as given by DFT are not. These apparently inconsistent results can be explained by remembering that the application of the BET or Langmuir method to isotherm data for microporous solids results in the attribution of the total micropore volume filling to free surface coverage. Whether this leads to over- or underestimation of the pore area depends on the pore dimensions. In fact, using simple geometric arguments, it can be shown that the area of pores less than about 3 molecular diameters in width will be underestimated, while the area of larger micropores will be greatly overestimated. We can assume that all the porosity smaller than 2 nm in an adsorbent will be filled at relative pressures less than 0.10 and, hence, will be included in the BET estimate of monolayer capacity. Let us assume, for example, that this micropore volume is 0.25 cm^3/g. Using the standard conversion parameters for the area occupied by a nitrogen molecule, the molar volume of nitrogen at 77 K, and Avogadro's number ($0.162\ \text{nm}^2 \times 0.0288 \times 6.023 \times 10^{23}$), this would be the equivalent to 702 m^2 of surface. From simple geometrical arguments, it can be shown that the surface area, A, of a cylindrical pore is given by $A = 4V/w$, where V is the pore volume and w is the width (diameter). If the pore size is taken as 0.74 nm, as in a faujasite, the above equation gives a specific surface area of 1350 m^2/g, much greater than 702. If the micropore size is as large as 2.0 nm, then the area would be only 500 m^2/g, significantly less than 702 m^2/g. Only for pores of 1.42 nm are the areas equal. The Langmuir and BET formalisms are based on the model of adsorption on a free surface. The Langmuir model assumes the surface saturates after the first adsorbed layer, while the BET model presumes that multilayers can form at higher pressures. However, neither model allows for the filling of micropores. Surface areas derived from these two models will differ from the actual area in a way that depends on the solid microporous structure. In the case of FCCs where both micro- and mesopores are present, the surface area determined from DFT will also be dependent on the geometry of the pore model used. The initial DFT models were developed for the study of activated carbons and were based on an assumed slit-pore geometry which generates a much smaller pore area for a given pore volume. This has led to the

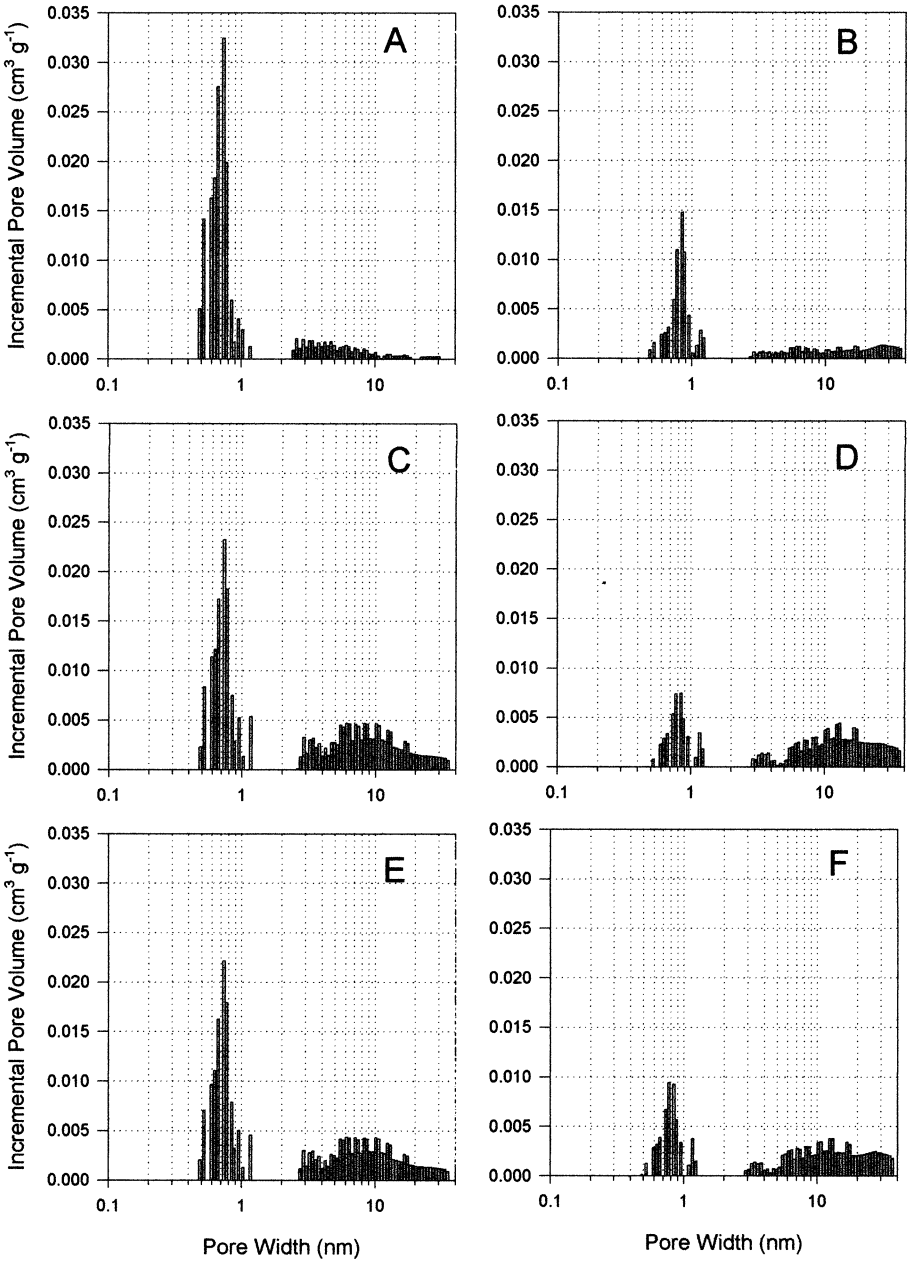

Figure 6. Incremental PV distribution data obtained by fitting the DFT model to sorption isotherms: (A) fresh FCC-A; (B) equilibrium FCC-A; (C) fresh FCC-B; (D) equilibrium FCC-B; (E) fresh FCC-C; (F) equilibrium FCC-C.

TABLE 3: Surface Area (SA, m^2/g) and Pore Volume (PV, cm^3/g) Results from Nitrogen Porosimetry Data for the FCC-A Sample

	fresh FCC-A				equilibrium FCC-A			
method	micro. SA	total SA	micro. PV	total PV[a]	micro. SA	total SA	micro. PV	total PV[a]
DFT	892	931	0.150	0.215	321	341	0.064	0.168
Langmuir		379				169		
BET		356				159		
t-plot	261	356	0.105		114	159	0.046	
HK			0.135				0.062	
D−R	410		0.145		226		0.080	

[a] Total PV data measured at $P/P_0 = 0.995$.

generation of FCC results in which surface areas were probably underestimated.[16] In the current work, a cylindrical pore model is used that avoids this problem.

Results in Tables 3−5 indicate that for microporous solids such as FCCs neither the BET nor the Langmuir method can adequately represent the catalyst surface area. The *t*-plot method is designed to determine micropore volume, and the data in Tables 3−5 show PV values in reasonable agreement with those from DFT calculations. Like the *t*-plot method, the D−R technique[6] is meant to determine total micropore volumes. While empirical, the results for total pore volume are in good agreement with DFT data (Tables 3−5). However, the D−R and *t*-plot methods give SA values that are unacceptably lower than those from DFT calculations; see Tables 3−5. Similarly,

TABLE 4: Surface Area (SA, m^2/g) and Pore Volume (PV, cm^3/g) Results from Nitrogen Porosimetry Data for the FCC-B Sample

	fresh FCC-B				equilibrium FCC-B			
method	micro. SA	total SA	micro. PV	total PV[a]	micro. SA	total SA	micro. PV	total PV[a]
DFT	654	729	0.115	0.299	218	262	0.044	0.238
Langmuir		312				132		
BET		298				128		
t-plot	142	298	0.059		51	128	0.021	
HK			0.115				0.049	
D−R	344		0.122		158		0.056	

[a] Total PV data measured at $P/P_0 = 0.995$.

TABLE 5: Surface Area (SA, m^2/g) and Pore Volume (PV, cm^3/g) Results from Nitrogen Porosimetry Data for the FCC-C Sample

	fresh FCC-C				equilibrium FCC-C			
method	micro. SA	total SA	micro. PV	total PV[a]	micro. SA	total SA	micro. PV	total PV[a]
DFT	612	680	0.108	0.283	264	307	0.052	0.248
Langmuir		299				153		
BET		284				145		
t-plot	140	284	0.058		68	145	0.028	
HK			0.110				0.056	
D−R	333		0.118		185		0.066	

[a] Total PV data measured at $P/P_0 = 0.995$.

TABLE 6: Ammonia Chemisorption Data at 150 °C[a]

					pop. of sites with a gn strength			
	init H	int H	V_T	V_{irr}	<100	100−120	120−140	>140
fresh FCC-A	153	70.3	631	415	181	260	161	29
fresh FCC-B	133	38.8	358	189	150	50	158	0
fresh FCC-C	151	36.8	339	179	135	75	104	25
equilibrium FCC-A	128	4.5	79	29	68	5	6	0
equilibrium FCC-B	104	5.2	85	23	70	15	0	0
equilibrium FCC-C	145	8.1	107	35	78	14	9	6

[a] $p = 0.2$ Torr. Initial heats (init H) are in kJ/mol. Integral heats (int H) are in J/g. V_T, V_{irr}, and the population of sites with a given strength are in μmol of NH_3/g.

the HK method can describe the microporous structure of FCCs by giving PV values in good agreement with micropore PV data determined by DFT but cannot provide information on the solids' SA; Tables 3−5. DFT results in these tables report that, in a refinery FCCU, a fresh FCC suffers a loss in total PV and SA that can be safely assigned to a partial loss of crystallinity of its cracking component and, possibly, to metals' (Fe, Ni, V) deposition during gas oil cracking. Evidence of pore blockage by these metals was not observed.

Microcalorimetry Results. Although microcalorimetry cannot distinguish betwen Bronsted and Lewis acidity, it can relate site strength to the nature of the sites present.[17,28] In zeolites, the strong sites (>160 kJ/mol) observed at low NH_3 coverage have been attributed to Lewis centers resulting from extraframework Al species produced during thermal and hydrothermal treatments. Sites of intermediate strength (i.e., 130−160 kJ/mol) of adsorption have been associated with Bronsted centers resulting mainly from bridging hydroxyls. Heat of adsorption in the 100−130 kJ/mol range represents weak Lewis sites, and below 100 kJ/mol, what is observed is the interaction of the probe molecule with weak silanol groups.[17,28,29]

Microcalorimetry results with ammonia as the probe molecule have been reported in Table 6 and in Figures 7−9. Chemisorption isotherms are shown in Figure 7. The higher chemisorption capacity exhibited by the FCC-A sample can be safely attributed to the catalyst's higher (~30 wt %) zeolite content. However, all three FCC samples undergo losses in acidity while in use in a FCCU, so that, irrespective of their composition, the chemisorption capacity in equilibrium FCC samples is reduced to

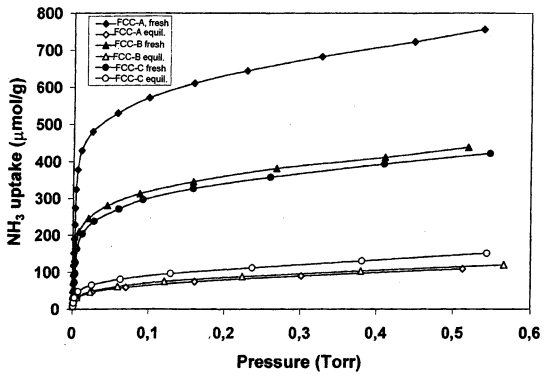

Figure 7. Ammonia chemisorption isotherms at 150 °C for the fresh and equilibrium FCC samples.

comparable levels (Figure 7). Not shown are secondary sorption isotherms, that is, sorption isotherms for samples after NH_3 adsorption and degassing in a vacuum at 150 °C. By subtracting the adsorbed volume of the secondary isotherms from that of the primary isotherms at the same equilibrium pressure (P = 0.2 Torr), it is possible to obtain V_{irr}, the volume of irreversibly chemisorbed sorbate. This value is believed to correlate with the presence of strong acid sites.[18,19] In Table 6, initial heats have been associated with the strength of the strongest acid sites present. On the other hand, integral heats represent the total heat of adsorption evolved at $P = 0.2$ Torr and are therefore associated with the solid's acid site density. The decrease in initial heats and NH_3 sorption, together with the decrease in integral heats of NH_3 chemisorption shown in Figure 8, reflects

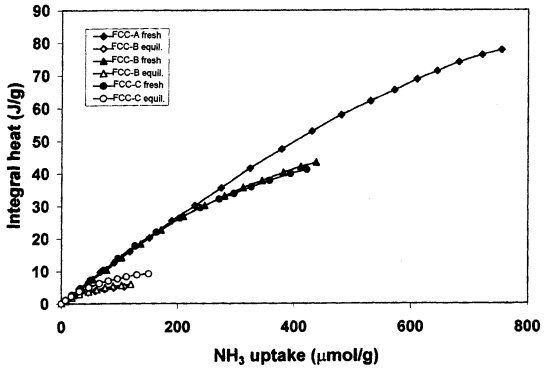

Figure 8. Integral heat profiles at $p = 0.2$ Torr for the fresh and equilibrium FCC samples.

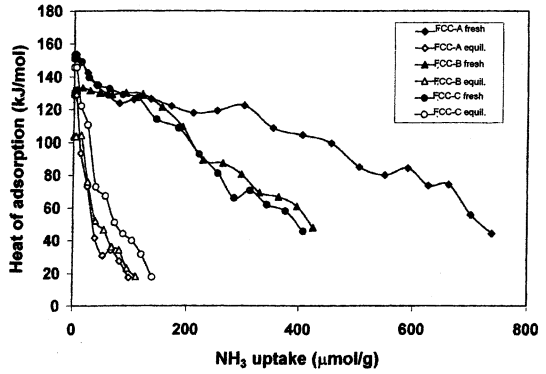

Figure 9. Differential heat profiles for the fresh and equilibrium FCC samples.

the loss of surface area and crystallinity that fresh FCCs experience in a FCCU. Similar results have been obtained while studying a FCC sample having different composition.[26]

The corresponding differential heats of ammonia adsorption as a function of coverage are shown in Figure 9. When using ammonia, in addition to some strong Lewis sites with strength near 155 kJ/mol, the fresh FCCs contain a population of sites, with strength near 133 kJ/mol, attributed to the FCC acidic component, which in this case is an HY type zeolite (20−30 wt %) stabilized by a low level of RE cations; see Table 1. The presence of an aluminosilicate matrix as in the sample FCC-A increases the initial overall acidity of the fresh catalyst (Figure 9). As observed in other FCCs,[16,30] after aging there is a sharp decrease in FCC acidity that can be safely attributed to losses of Si(OH)Al groups in the zeolites and in the matrix.[16] Aging in a typical FCCU induces a drastic loss in acid sites' density, leaving a porous structure containing an heterogeneous distribution of sites' strength; the strength of these sites monotonically decreases with NH_3 coverage; see Table 6 and Figure 9. The strength of the strongest sites in these three FCCs is in the 100−145 kJ/mol range while the number of strong sites (as determined by Virr) is between 70 and 110 μmol of NH_3/g, indicating that neither strong Lewis sites nor a high density of strong acid sites is required for gas oil cracking; see Tables 2 and 6.

Comments

The determination of acidity in solids from adsorption microcalorimetry experiments with ammonia as the probe molecule remains a subject of controversy and debate.[30,31] It has been long recognized that a strong base such as ammonia is too readily adsorbed on strong as well as weak acid sites resulting from anionic vacancies, not fully coordinated metal ions (Lewis sites), or M−OH centers (Bronsted sites), thus providing acidity data that may not correlate with the solid catalytic activity. On the other hand, a weak base such as pyridine is expected to react only with strong acid sites, that is, with sites that are more likely to contribute to the solid's reactivity. Unfortunately, pyridine is a highly toxic liquid and its use has been curtailed by environmental regulation and protocols. Other probe molecules such as amines have been proposed.[32] In the case of FCCs of the type described in this paper, it has been shown that ammonia and pyridine yield consistent results with respect to ranking catalysts in order of acidity, acid sites' density, and strength.[16] Moreover, the dependence of the acidic properties of faujasites on framework composition can be adequately studied by using either FTIR spectra of chemisorbed pyridine or adsorption microcalorimetry experiments with NH_3.[33] Thus, although ammonia may not be recommended as a probe molecule in characterization techniques such as TPD,[32] it can provide useful microcalorimetry data.[16,18,19] A recent review of this technique to characterize solid acids is in ref 33.

Summary and Conclusions

During gas oil conversion in a refinery FCCU, metal impurities' (such as Ni, V, Fe) and passivating agents' (such as Sb and Sn) deposits will depend on feedstock quality and catalyst properties as well as on reactor conditions. Evidence of preferential metals' deposition near the FCC pore's mouth and suppression of active surface area from the cracking process was not observed in the three FCCs under study. DFT results in Tables 3−5 report that, after gas oil cracking, the fresh FCCs suffer a loss in total PV and SA that can be safely assigned to the partial loss of crystallinity of the FCCs' cracking component and, possibly, to metals' (Fe, Ni, V) deposition during gas oil cracking. As a result, there is a drastic reduction in acid site strength and density. Acid site density plays a minor role in FCC activity, and as long as Lewis type sites with strength greater than 100 kJ/mol are present and as long as these sites are available to gas oil cracking, the FCC will maintain its useful cracking activity. These results lend support to the possibility that gas oil cracking is initiated by hydride abstraction on L-sites with formation and cracking of carbenium ions.[16]

Both the BET and Langmuir equations grossly underestimate the FCC total surface area while other traditional methods such as the *t*-plot, DR, and HK methods cannot provide PV and SA distribution data over the catalyst's entire micro−meso range. To elucidate the unique porous structure of current FCCs, a method based on molecular scale statistical thermodynamics is needed. The NLDFT provides such a method and allows us to extract from adsorption data a much more complete description of the porous catalyst than that from traditional methods.

Acknowledgment. This work has been supported in part by NATO collaborative grant CRG-971497 to M.L.O. Special thanks are due to Mr. M. Victor and Mr. J. Gonzales (Akzo Nobel) for providing FCC samples and MAT results.

References and Notes

(1) Wolf, E. H.; Alfani, A. Catalyst Deactivation by Coking. *Catal. Rev. Sci. Eng*. **1982**, *24*, 329 and references therein.

(2) Trimm, D. L. In *Progress in Catalysts Deactivation*; Figueiredo, J. L., Ed.; Nijhoff: TheHague/Boston/London, 1982; p 65.

(3) Barret, E. P.; Joyner, L. S.; Halenda, P. P. *J. Am. Chem. Soc*. **1951**, *73*, 373−380.

(4) Langmuir, I. *J. Am. Chem. Soc*. **1916**, *38*, 2221; *Phys. Rev*. **1916**, *8*, 149.

(5) Brunauer, S.; Emmett, P. H.; Teller, E. *J. Am. Chem. Soc*. **1938**, *60*, 309−319.

(6) Dubinin, M. M.; Radushkevich, L. V. *Proc. Acad. Sci., Phys. Chem. Sect., USSR* **1947**, *55*, 331−333.

(7) DeBoer, J. H.; Linse, B. G.; Osinga, Th. J. *J. Catal*. **1965**, *4*, 643−648.

(8) Lippens, B. C.; De Boer, J. H. *J. Catal*. **1965**, *4*, 319−323.

(9) Brunauer, S.; Mikhail, R. Sh.; Bodor, E. E. *J. Colloid Interface Sci*. **1967**, *24*, 451−463.

(10) Horvath, G.; Kawazoe, K. *J. Chem. Eng. Jpn.* **1983**, *16*, 470.

(11) Saito, A.; Foley, H. C. *AIChE J.* **1991**, *37*, 429−436.

(12) Roquerol, F.; Rouquerol, J.; Sing, K. *Adsorption by Powders and Porous Solids*; Academic Press: London, 1999; p 232.

(13) Olivier, J. P.; Occelli, M. L. *J. Phys. Chem. B* **2001**, *105* (3), 623−629.

(14) Tarazona, P. *Phys. Rev A* **1985**, *31*, 2672−2679; *Phys. Rev. A* **1985**, *32*, 3148 (Erratum).

(15) Tarazona, P.; Marconi, U. M. B.; Evans, R. *Mol. Phys*. **1987**, *60*, 573−595.

(16) Occelli, M. L.; Eckert, H.; Wolker, A.; Kalwei, M.; Auroux, A.; Gould, S. *J. Catal*. **2000**, *196*, 134−148.

(17) Auroux, A.; Ben Taarit, Y. *Thermochim. Acta* **1987**, *122*, 63.

(18) Auroux, A. In *Catalyst Characterization: Physical Techniques for Solid Materials*; Imelik, B., Vedrine, J. C., Eds.; Plenum Press: New York, 1994; Chapter 22.

(19) Auroux, A. *Top. Catal.* **1997**, *4*, 71−89.

(20) Occelli, M. L. In *Catalysts in Petroleum and Petrochemical Industries*; Absi-Halabi, M., Beshara, J., Qabazard, H., Stanislaus, A., Eds.; Elsevier: 1996; p 27.

(21) Olivier, J. P.; Conklin, W. B. Determination of pore size distribution from density functional theory models of adsorption and condensation within pores. Presented at the *First International Symposium on Effects of Surface Heterogeneity in Adsorption and Catalysis on Solids*, Kazimierz Dolny, Poland, 1992.

(22) Olivier, J. P. *J. Porous Mater*. **1995**, *2*, 9−17.

(23) Olivier, J. P.; Koch, S.; Jaroniec, M.; Kruk, M. *Characterization of porous solids V*; Studies in Surface Science, vol. 128; Unger, K. K., et al., Eds.; Elsevier: Amsterdam, 2000; p 71.

(24) Seaton, N. A. *Carbons* **1989**, *27*, 853.

(25) Lastoski, C. M.; Gubbins, K. E.; Quirke, N. *J. Phys. Chem*. **1993**, *97*, 4786.

(26) Occelli, M. L.; Olivier, J. P.; Auroux, A. *J. Catal*. **2002**, *209*, 385−393.

(27) Occelli, M. L.; Baldiraghi, F.; Gould, S. A. C.; Leoncini, S. In *Fluid Cracking Catalysts*; Occelli, M. L., O'Connor, P., Eds.; Marcel-Dekker: 1998; p 227.

(28) Shi, Z. C.; Auroux, A.; Ben Taarit, Y. *Can. J. Chem.* **1988**, *66*, 1013.

(29) Cardona-Martinez, N.; Dumesic, J. A. *J. Catal*. **1990**, *125*, 427.

(30) Juskelis, M. V.; Slanga, J. P.; Roberi, T. G.; Peters, A. W. *J. Catal*. **1992**, *138*, 391.

(31) Gorte, R. J. *Catal. Lett.* **1999**, *62*, 1−13.

(32) Gricus, T. J.; Kofke, R. J.; Gorte, R. J.; Farneth, W. E. *J. Catal*. **1988**, *114*, 34.

(33) Auroux, A. *Top. Catal.* **2002**, *19* (3−4), 205−213.